Charge order, orbital order, and electron localization in the Magnéli phase Ti4O7

Volker Eyert, Udo Schwingenschlögl, Ulrich Eckern

Angaben zur Veröffentlichung / Publication details:

Eyert, Volker, Udo Schwingenschlögl, and Ulrich Eckern. 2004. "Charge order, orbital order, and electron localization in the Magnéli phase Ti4O7." *Chemical Physics Letters* 390 (1-3): 151–56. https://doi.org/10.1016/j.cplett.2004.04.015.

Charge order, orbital order, and electron localization in the Magnéli phase Ti_4O_7

V. Eyert *, U. Schwingenschlögl, U. Eckern

Institut für Physik, Universität Augsburg, Universitätsstrasse 1, 86135 Augsburg, Germany

Abstract

The metal–insulator transition of the Magnéli phase Ti_4O_7 is studied by means of augmented spherical wave (ASW) electronic structure calculations as based on density functional theory and the local density approximation. The results show that the metal–insulator transition arises from a complex interplay of charge order, orbital order, and singlet formation of those Ti 3d states which mediate metal–metal bonding inside the four-atom chains characteristic of the material. Ti_4O_7 thus combines important aspects of Fe_3O_4 and VO_2. While the charge ordering closely resembles that observed at the Verwey transition, the orbital order and singlet formation appear to be identical to the mechanisms driving the metal–insulator transition of vanadium dioxide.

1. Introduction

Since the seminal work of Morin [1] the metal–insulator transitions of the early transition-metal oxides are motivating ongoing research. In particular, showing first-order transitions with a conductivity change of several orders of magnitude, VO_2 and V_2O_3 are regarded as prototypical materials of this class. Recent theoretical work has revealed a strong influence via electron–phonon coupling of the structural degrees of freedom on the electronic properties of VO_2 and neighbouring rutile-type dioxides [2–5]. In contrast, the corundum-type sesquioxide has turned out to be subject to strong electronic correlations [6,7], as seems to be the case also for Ti_2O_3 [8]. The relative importance of these mechanisms as well as their dependence on crystal structure and band filling are still unclear.

In this situation the Magnéli phases offer the opportunity of a more comprehensive understanding [9]. These phases form a homologous series of the kind M_nO_{2n-1} (M = Ti, V) and are particularly suited for studying the differences in crystal structures and electronic properties between the end members MO_2 ($n \to \infty$) and M_2O_3 ($n = 2$). This is due to the variation in d band occupation across the series as well as the fact that, as the general formula $M_nO_{2n-1} = M_2O_3 + (n-2)\ MO_2$ suggests, the crystal structures can be viewed as rutile-type slabs of infinite extension and different thickness, separated by shear planes with a corundum-like atomic arrangement [9]. While in the rutile-type regions the characteristic metal–oxygen octahedra are coupled via edges, the shear planes have face-sharing octahedra as in the corundum structure. We have recently started a systematic investigation of the vanadium Magnéli phases [10–13]; here we report on the first results for the titanium series.

The Magnéli phase Ti_4O_7 experiences a metal–insulator transition at 154 K, which is followed by an insulator–insulator transition at 130 K with a thermal hysteresis of about 12 K [14–16]. Both transitions are first-order [15–17] and connected with a conductivity change of three orders of magnitude each [14]. While a sharp decrease of the magnetic susceptibility has been reported for the 154 K transition, which has been interpreted as a change from Pauli paramagnetism to van Vleck-like behaviour [16], there is no considerable change at lower temperatures [14,18]. In contrast,

* Corresponding author. Fax: +49-821-598-3262.
E-mail address: eyert@physik.uni-augsburg.de (V. Eyert).

whereas the transition at 154 K goes along with increase in volume [17], a distortion of the crystal structure had been first observed only for the second transition [14]. From single-crystal X-ray diffraction data taken at 298, 140, and 120 K, Marezio et al. [17,19,20] reported differentiation of the Ti–O distances on going to the low-temperature phase, suggesting the formation of Ti^{3+} and Ti^{4+} sites, which each occupy half of the characteristic four-atom chains and which contrast the average $Ti^{3.5+}$ valence observed at high temperatures. In addition, the Ti^{3+} sites form short metal–metal bonds indicating singlet formation and explaining the changes in resistivity and magnetic susceptibility. At the same time the unpaired Ti^{4+} and, to a lesser degree, the Ti^{3+} atoms are displaced perpendicular to the chain axis off the center of the surrounding octahedron towards one of the oxygen atoms [17,19,20]. This pattern is similar to the situation found for Cr-doped VO_2, where half of the chains pair and atoms on the remaining chains display a zigzag-like off-center displacement [3]. Finally, Marezio et al. reported large thermal displacements for the intermediate phase, suggesting that the structural changes are associated with the metal–insulator transition at 154 K but still lack long-range order [17,20]. The latter sets in at the lower transition, which is thus regarded as a disorder–order transition [17,20] as has been confirmed by specific-heat and EPR data [15,16]. These results led to interpret the intermediate phase as a bipolaron liquid [15,16,21]. Yet, refined determination of the crystal structure revealed a fivefold superstructure for the intermediate phase, which shows the same structural characteristics as the low-temperature phase, and thus questioned understanding the conductivity in terms of independent mobile bipolarons [22]. Recent photoemission and X-ray absorption measurements showed only minor effects of the insulator–insulator transition on the electronic properties but revealed drastic changes at 154 K [23,24]. The latter include significant down- and upshift of the occupied and unoccupied Ti 3d t_{2g} states near the Fermi energy. In contrast, O 2p states extending from -9 to -4 eV remain essentially unaffected by the transition.

Understanding of the physical properties of the Magnéli phases is greatly facilitated by an alternative unified representation of their crystal structures [10–13,17,20]. It is based on the notion of a hexagonal closed-packed array of oxygen atoms forming a regular 3D network of octahedra. Apart from a slightly different buckling, this network is the same for all Magnéli phases including the rutile-type dioxide and the corundum-type sesquioxide. Differences between the compounds Mn_nO_{2n-1} arise from filling the octahedra with metal atoms. Filled octahedra form chains of length n parallel to the pseudorutile c_{prut}-axis, followed by $n-1$ empty sites. While in the rutile structure these chains have infinite length, they comprise just two filled octahedra in the corundum structure, where they are perpendicular to the hexagonal c-axis. Within the crystal, the metal chains are arranged in two different types of layers, which are interlaced by oxygen layers and alternate along a_{prut}. This gives rise to the aforementioned two types of chains, labelled (a) and (b). In Ti_4O_7, they comprise atoms Ti1/Ti3 and Ti2/Ti4, respectively (see Fig. 1 of [11], where this situation has been sketched for the isostructural V_4O_7). Due to alternation of the layers and relative shifts of the four-atom chains within the layers the end atoms Ti1 and Ti2 are found on top of each other (note that in the notation by Marezio et al. [17,20] the chain center and end atoms are reversed). In the sesquioxide, these two atoms are usually designated as the c-axis pair. While neighbouring octahedra share faces along a_{prut} and b_{prut}, metal–metal bonding along all other directions within the layers is via edges [3]. As a consequence, the atomic arrangement near the chain ends is corundum-like, whereas the chain centers correspond to the rutile-type regions. By virtue of the just sketched representation of the crystal structures it is possible to refer the symmetry components of the Ti 3d orbitals of all compounds to a common local coordinate system [3]. In this system the z- and x-axes of the local coordinate system are parallel to the apical axis of the local octahedron and the pseudorutile c_{prut} axis, respectively.

In this Letter, we report on electronic structure calculations for the Magnéli phase Ti_4O_7 using the crystal structures of both the room-temperature and the low-temperature phase. Our calculations reveal: (i) rather isotropic occupation of the Ti 3d t_{2g} states for the room-temperature structure, (ii) significant electron transfer from one half of the chains to the other in the low-temperature structure, (iii) orbital order at the d^1 chains coming with strong metal–metal dimerization, and iv) strong electron localization, which leads the way to the observed metal–insulator transition.

2. Methodology

The calculations were performed using the scalar-relativistic augmented spherical wave (ASW) method [25,26]. In order to represent the correct shape of the crystal potential in the large voids of the open crystal structure, additional augmentation spheres were inserted. Optimal augmentation sphere positions as well as radii of all spheres were automatically generated by the sphere geometry optimization (SGO) algorithm [27]. Self-consistency was achieved by an efficient algorithm for convergence acceleration [28]. Brillouin zone sampling was done using an increased number of k-points ranging from 108 to 2048 points within the irreducible wedge.

3. Results and Discussion

Calculated partial densities of states (DOS) are displayed in Fig. 1. Here and in all following figures results for the room-temperature and low-temperature structure are given on the left and right, respectively. In Fig. 1, contributions from both the Ti 3d and O 2p states are included. In addition, Ti contributions from the (a) and (b) chains containing Ti1/Ti3 and Ti2/Ti4, respectively, are distinguished. All other orbitals play only a negligible role in the energy interval shown.

Two groups of bands are identified, which extend from −0.5 to 2.0 eV and from 2.4 to 4.6 eV and comprise 24 and 16 bands, respectively. They derive mainly from the Ti 3d states. In addition, 42 bands are found in the energy range from −8.5 to −3.8 eV, which trace back mainly to the O 2p states. However, p–d hybridization causes d and p contributions, respectively, below and above −2 eV reaching about 15% especially in the two upper groups. Crystal field splitting expected from the fact that the Ti atoms are located at the centers of slightly distorted octahedra is observed in the Ti 3d partial DOS. As a detailed analysis of the wave functions reveals, the lower group of Ti 3d derived bands arises almost exclusively from states of t_{2g} symmetry. In contrast, bands between 2.4 and 4.6 eV trace back to the e_g states. The energetical separation of the centers of gravity of these two groups of about 2.7 eV compares well with the value of 2.4 eV taken from the XAS measurements by Abbate et al. [23]. At the same time, the calculated position and width of the O 2p dominated group of bands is in very good agreement with the photoemission data of these authors.

In general, these findings are very similar for the room-temperature and the low-temperature structure. In particular, the O 2p bands keep their energetical position and band width, again in agreement with the photoemission data [23]. Differences show up on closer inspection of the Ti 3d dominated states. Most striking are the changes occurring in the occupied part of the Ti 3d t_{2g} bands. While for the room-temperature structure the Ti 3d partial DOS in this energy interval are almost the same for both chains, we observe strong increase and decrease of the Ti 3d partial DOS arising from the atoms of chain (a) and (b), respectively, for the low-temperature structure indicative of a considerable charge transfer. The integrated difference amounts to ≈0.8 electrons per formula unit. At the same time, states in the Ti 3d e_g group of bands, i.e., between 2.4 and 4.6 eV, experience some rearrangement. In particular, on going from the room-temperature results to those obtained for the low-temperature structure, we find energetical down- and upshift, respectively, of the centers of gravity of these bands for chain (a) and (b).

Both these changes can be attributed to the difference of the average Ti–O distances emerging in the low-temperature phase [17]. They lead to the assignment of Ti d^0 and d^1 charges contrasting the formal $d^{0.5}$ valence of the room-temperature phase [17]. While in the latter phase the average Ti–O bond length is the same for all titanium sites, in the low-temperature phase the average bond length increases and decreases for chain (a) and (b) atoms, respectively. As a consequence, d electron charge is transferred from atoms Ti2/Ti4 to Ti1/Ti3, leaving the d states in the (b) chains unoccupied. In addition, the shrinking and inflating of the oxygen octahedra strongly affect the bonding–antibonding splitting especially of the σ-bonding states of e_g symmetry. This splitting decreases/increases in chains (a)/(b), leading to the observed down-/upshift of the Ti 3d dominated antibonding states.

In order to investigate the charge redistribution coming with the transitions in more detail we display the Ti 3d t_{2g} partial DOS of all four titanium atoms separately in Figs. 2 and 3. In doing so we distinguish the three different d states contributing to this group of bands using the aforementioned local coordinate system as defined in [3]. In this system, the $d_{x^2-y^2}$ states, pointing parallel to the pseudorutile c_{prut} axis, mediate σ-type metal–metal overlap within the chains. In

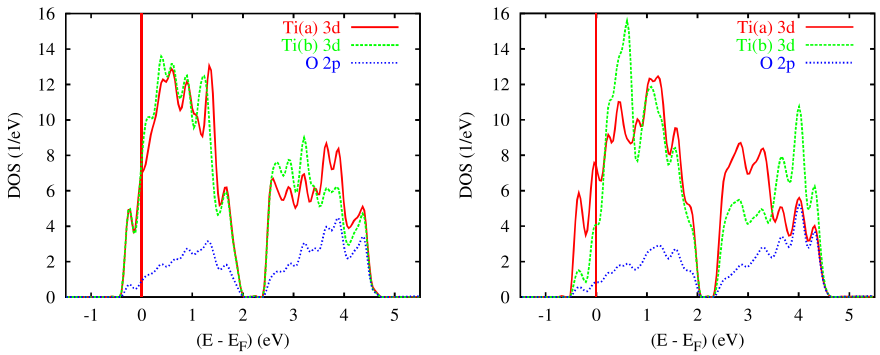

Fig. 1. Partial DOS as resulting from the room-temperature (left) and low-temperature (right) crystal structure. Here and in the following figures slight broadening is due to the DOS calculation scheme [29].

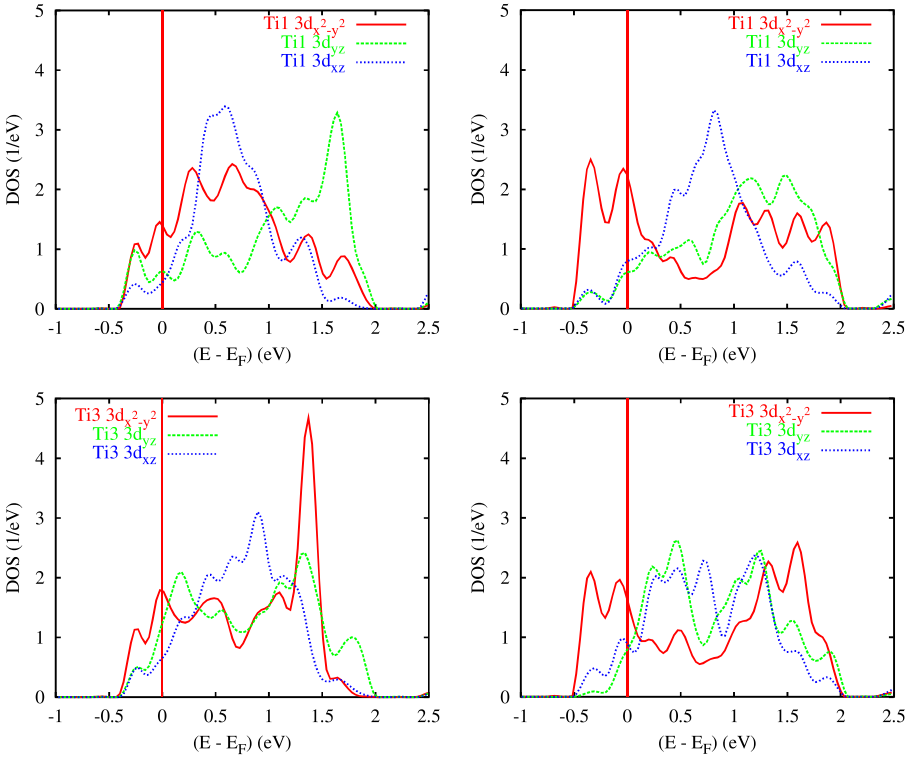

Fig. 2. Partial 3d t_{2g} DOS of (a) chain atoms Ti1 and Ti3.

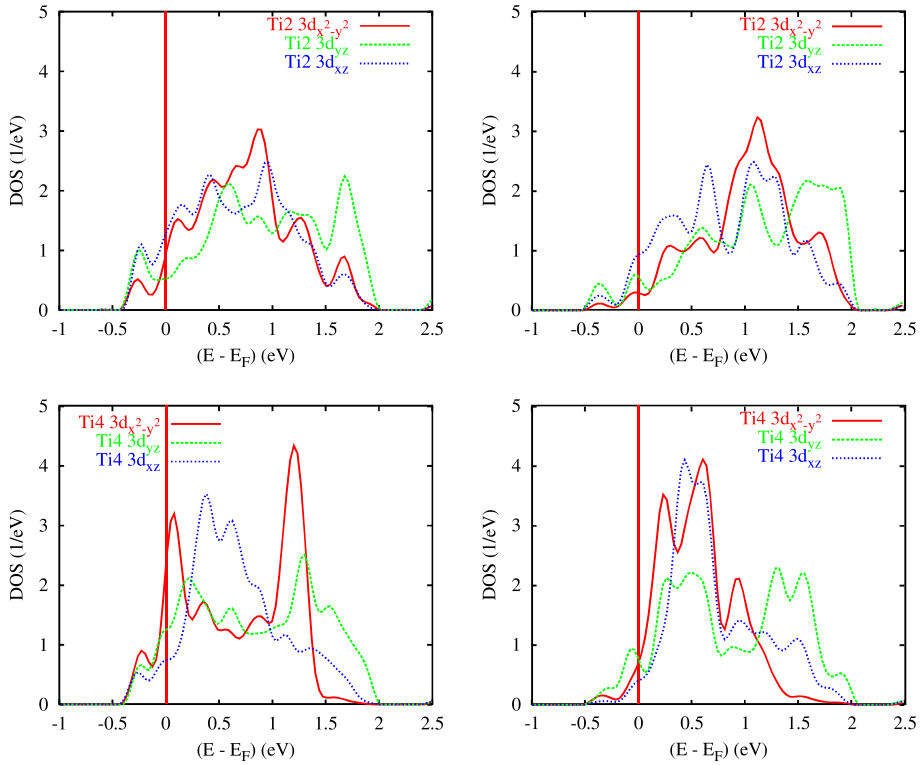

Fig. 3. Partial 3d t_{2g} DOS of (b) chain atoms Ti2 and Ti4.

contrast, the d_{yz} orbitals take part in albeit weaker σ-type d–d overlap across the chains. Weak interchain coupling is also due to overlap of $d_{x^2-y^2}$ and d_{xz} orbitals of neighbouring chains.

For the high-temperature structure strong splitting of the $d_{x^2-y^2}$ states of both Ti3 and Ti4 is observed. This is a consequence of the short Ti3–Ti3 and Ti4–Ti4 distances in the chain centers causing strong bonding–antibonding splitting of the $d_{x^2-y^2}$ orbitals of these atoms. In contrast, distances between the chain center and end atoms are considerably larger, this leading to the somewhat unstructured shape of the $d_{x^2-y^2}$ partial DOS of atoms Ti1 and Ti2. Similar shapes are displayed by the d_{xy} partial DOS of all atoms due to the very small metal–metal bonding these states take part in. Finally, the d_{yz} states of all atoms show distinct splitting into bonding and antibonding states, reflecting overlap of these orbitals of atoms Ti3 and Ti4 (peaks at 0.2 and 1.35 eV) as well as atoms Ti1 and Ti2. In the latter case overlap is parallel to the pseudorutile a_{prut} axis perpendicular to the chains across octahedral faces. This bond corresponds to the *c*-axis pairs in the sesquioxide. Indeed, the shape of the d_{yz} partial DOS with its pronounced antibonding peak at 1.6 eV and the tail of bonding states extending from −0.3 to 1.3 eV has been also observed for V_2O_3.

On going to the low-temperature phase several striking changes occur. First, we observe the above-mentioned increase and decrease of the partial DOS of the (a) and (b) chain atoms, respectively, in the occupied part of the spectrum, which is a consequence of the charge ordering coming with the increased and reduced average Ti–O bond-length as reported by Marezio and coworkers [17,20]. In the (b) chains smaller distances induce a stronger bonding–antibonding splitting of the hybridized Ti 3d and O 2p states, hence, upshift of the antibonding d dominated bands. This effect is supported by the displacement of these atoms perpendicular to the chains. Eventually, we witness almost complete depopulation of the (b) chain states, i.e., Ti d^0 valence. In contrast, on the (a) chains longer Ti–O distances lead to reduced bonding–antibonding splitting, hence, energetical lowering of the d bands and the occupation reaches nearly d^1.

Second, in addition to the charge ordering we find strong changes in the occupation of the single d states of the (a) chain atoms. Due to the albeit small displacement of atoms Ti1 and Ti3 perpendicular to the chain axis the d_{xz} and d_{yz} states of these atoms are subject to larger d–p hybridization and thus shift to higher energies. In contrast, both the Ti1 and Ti3 $d_{x^2-y^2}$ partial DOS show strong splitting into a double maxima structure with peaks near −0.25 and 1.5 eV. This effect results from the dimerization of these two atoms observed below the metal–insulator transition, which leads to metal–metal overlap of the orbitals extending along the (a) chains and splitting of the corresponding bands into bonding and antibonding states. At the same, chain (b) atoms do not display any splitting of these states due to the uniform distance of more than 3.0 Å between all atoms of this chain.

The corresponding changes of the band structure as shown in Fig. 4 have drastic effects especially near the Fermi energy. While in the room-temperature structure bands in the lower part of the t_{2g} group show strong dispersion leading to the metallic behaviour, the low-temperature structure is characterized by two split-off bands. As expected from the partial DOS and as revealed by a detailed analysis of the wave functions, these weakly dispersing bands are almost exclusively of Ti1 and Ti3 $d_{x^2-y^2}$ character. Additional bands of the same symmetry, which likewise show a reduced dispersion, are found at the upper edge of the t_{2g} group, supporting the previous interpretation in terms of bonding–antibonding splitting of these states. Yet, despite the separation of the lower $d_{x^2-y^2}$ bands from all higher lying states there is still a semimetal-like overlap of about 0.1 eV, inhibiting the complete opening of the insulating band gap.

In general, the situation resembles very much that found for the rutile-type compounds TiO_2 and VO_2, where the metal atoms are found in a d^0 and d^1 configuration, respectively. While the insulating titanate

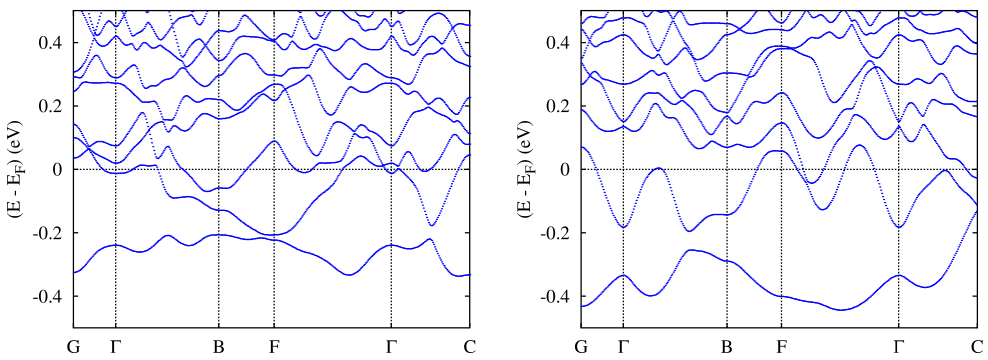

Fig. 4. Electronic band structure.

preserves the rutile structure down to lowest temperatures maintaining especially the equidistant spacing of the metal atoms, vanadium dioxide shows distinct deviations from this structure at the metal–insulator transition. In particular, vanadium atoms experience pairing parallel to the c_{rut} axis as well as zigzag-like antiferroelectric displacements perpendicular to this axis. In the calculation for VO_2, these changes lead to splitting of the $d_{x^2-y^2}$ bands as well as energetical upshift of the d_{xz} and d_{yz} states [3]. We may thus regard low-temperature Ti_4O_7 as composed of TiO_2- and VO_2-like chains, which display the same behaviour as the respective dioxide. Common to VO_2 and Ti_4O_7 is also the finding of a small semimetal-like overlap for the low-temperature phase, which we attribute to the shortcomings of the local density approximation. Yet, this weakness does not undermine the interpretation of the phase transitions of both compounds as arising from orbital order and strong bonding–antibonding splitting of the $d_{x^2-y^2}$ bands due to the structural changes and strong electron–phonon coupling. In addition, Ti_4O_7 is characterized by distinct charge ordering, leading to separated d^0 and d^1 chains and laying ground for the efficacy of the aforementioned mechanisms.

4. Conclusion

In summary, according to electronic structure calculations for the Magnéli phase Ti_4O_7, the metal–insulator transition of this material arises from the complex interplay of different types of ordering phenomena. While in the room-temperature structure all Ti 3d t_{2g} states display uniform occupation, the low-temperature structure is characterized by the formation of two types of titanium chains comprising Ti d^0 and d^1 states, respectively. This charge ordering is accompanied by orbital ordering on the d^1 chains and strong bonding–antibonding splitting of the respective $d_{x^2-y^2}$ states coming with Ti–Ti dimerization and zigzag-type antiferroelectric displacement of these atoms in complete accordance with the findings for the d^1 dioxide VO_2. Finally, like in the latter compound, singlet formation on the $d_{x^2-y^2}$ states paves the way for the observed insulating behaviour.

To conclude, Ti_4O_7 shares fundamental aspects with other cornerstone materials of condensed matter physics. The charge ordering occurring at the metal–insulator transition is closely related to that discussed for the Verwey transition of Fe_3O_4. In contrast, the orbital order and metal–metal dimerization accompanying the phase transition of Ti_4O_7 arise from the same mechanism as that driving the transitions of VO_2 and NbO_2, namely instability of the d^1 atom chains towards the strong metal–metal bonding along the characteristic chains as well as antiferroelectric displacement perpendicular. This effect may thus be regarded as a universal mechanism common to many early rutile-type transition-metal compounds.

Acknowledgements

This work was supported by the Deutsche Forschungsgemeinschaft (DFG) through Sonderforschungsbereich SFB 484.

References

[1] F.J. Morin, Phys. Rev. Lett. 3 (1959) 34.
[2] R.M. Wentzcovitch, W.W. Schulz, P.B. Allen, Phys. Rev. Lett. 72 (1994) 3389.
[3] V. Eyert, Ann. Phys. (Leipzig) 11 (2002) 650.
[4] V. Eyert, R. Horny, K.-H. Höck, S. Horn, J. Phys.: Condens. Matter 12 (2000) 4923.
[5] V. Eyert, Europhys. Lett. 58 (2002) 851.
[6] S.Yu. Ezhov, V.I. Anisimov, D.I. Khomskii, G.A. Sawatzky, Phys. Rev. Lett. 83 (1999) 4136.
[7] K. Held, G. Keller, V. Eyert, D. Vollhardt, V.I. Anisimov, Phys. Rev. Lett. 86 (2001) 5345.
[8] A.I. Poteryaev, A.I. Lichtenstein, G. Kotliar, cond-mat/0311319.
[9] S. Andersson, B. Collen, U. Kuylenstierna, A. Magnéli, Acta Chem. Scand. 11 (1957) 1641.
[10] U. Schwingenschlögl, V. Eyert, U. Eckern, Europhys. Lett. 61 (2003) 361.
[11] U. Schwingenschlögl, V. Eyert, U. Eckern, Europhys. Lett. 64 (2003) 682.
[12] U. Schwingenschlögl, Ph.D. thesis, Universität Augsburg, 2004.
[13] U. Schwingenschlögl, V. Eyert, Ann. Phys. (Leipzig) 13 (2004), in press.
[14] R.F. Bartholomew, D.R. Frankl, Phys. Rev. 187 (1969) 828.
[15] C. Schlenker, S. Lakkis, J.M.D. Coey, M. Marezio, Phys. Rev. Lett. 32 (1974) 1318.
[16] S. Lakkis, C. Schlenker, B.K. Chakraverty, R. Buder, M. Marezio, Phys. Rev. B 14 (1976) 1429.
[17] M. Marezio, D.B. McWhan, P.D. Dernier, J.P. Remeika, Phys. Rev. Lett. 28 (1972) 1390.
[18] L.N. Mulay, W.J. Danley, J. Appl. Phys. 41 (1970) 877.
[19] M. Marezio, P.D. Dernier, J. Solid State Chem. 3 (1971) 340.
[20] M. Marezio, D.B. McWhan, P.D. Dernier, J.P. Remeika, J. Solid State Chem. 6 (1973) 213.
[21] C. Schlenker, M. Marezio, Phil. Mag. B 42 (1980) 453.
[22] Y. Le Page, M. Marezio, J. Solid State Chem. 53 (1984) 13.
[23] M. Abbate, R. Potze, G.A. Sawatzky, C. Schlenker, H.J. Lin, L.H. Tjeng, C.T. Chen, D. Teehan, T.S. Turner, Phys. Rev. B 51 (1995) 10150.
[24] K. Kobayashi, T. Susaki, A. Fujimori, T. Tonogai, H. Takagi, Europhys. Lett. 59 (2002) 868.
[25] A.R. Williams, J. Kübler, C.D. Gelatt Jr., Phys. Rev. B 19 (1979) 6094.
[26] V. Eyert, Int. J. Quantum Chem. 77 (2000) 1007.
[27] V. Eyert, K.-H. Höck, Phys. Rev. B 57 (1998) 12727.
[28] V. Eyert, J. Comp. Phys. 124 (1996) 271.
[29] M. Methfessel, A.T. Paxton, Phys. Rev. B 40 (1989) 3616.